

A MODEL FOR HEAT FLUX ON A CYLINDRICAL TARGET DUE TO THE IMPINGEMENT OF A LARGE-SCALE NATURAL GAS JET FIRE

R.F. Cracknell, J.N. Davenport and A.J. Carsley

Shell Research Limited, Thornton Research Centre, P.O. Box 1, Chester, CH1 3SH

© Shell Internationale Research Maatschappij B.V. 1995

A model has been developed to describe the heat flux distribution for large-scale natural gas jet fires directly impinging on cylindrical objects. The model was parameterised using experimental data generated at the Spadeadam test site. Natural gas flames are optically thin, but for flames of length 20-30 m, radiation makes a substantial contribution to the overall flux. The model therefore treats the flame as an ensemble of cylinders, the distribution of which is described by a flame probability model and the radiation from each cylinder is calculated by numerical integration. A correlation has been developed for the variation of the convective heat transfer coefficient with distance from the release; this correlation is independent of release velocity. The ability of the flame to spread out along the target from its impingement point has also been addressed using a physically based model. The model is shown to give reasonable agreement with experimental data, both for contour plots of total heat flux density and also for plots of impinged area versus heat flux. Where there are discrepancies, the model makes a conservative prediction of the heat flux density.

Key Words: Natural Gas, Jet Fire, Impingement, Heat Flux, Radiation, Convection

INTRODUCTION

A release of pressurised flammable hydrocarbon may result in a jet fire. The origins of such a fire may either be deliberate e.g. flares on oil rigs, or results from the accidental rupture of storage vessels, or pipelines. Uncontrolled jet fires may pose a considerable threat to both life and property: impingement of a jet fire on an offshore structure may cause weakening with possible disastrous consequences: alternatively impingement of a jet fire on another pipe or storage tank may lead to escalation, e.g. a BLEVE. An understanding of the hazards associated with large-scale hydrocarbon jet fires is therefore important for the safe design and operation of process plants and storage facilities as well as for offshore installations.

To meet these needs, Shell Research has carried out a comprehensive programme of full-scale jet fires using a purpose-built jet fire facility at the British Gas test site at Spadeadam in Cumbria. Tests have been carried out for both freely burning flames as well as flames impinging onto cylindrical objects (a hydrocarbon storage tank and a pipe)<sup>1,2</sup>. For free flames, a model has been developed for predicting both flame shape and external radiation as a function of general release orientations and weather conditions for both propane and natural gas jet flames<sup>3,4</sup>. More recently, Carsley has used computer-based image processing techniques to analyse frame by frame, video records of horizontally released propane and natural gas free flames from the Spadeadam tests, together with vertically released laboratory-scale natural gas flames, in order to construct a model which can describe the probability of flame occurrence at a given point in space. This model, described separately at this symposium, can be used to calculate the probability with which a jet flame from a given release will impinge on particular objects in the vicinity of the release<sup>5</sup>. Quantification of the hazard, however, requires, in addition to the impingement probability, a model for the heat flux associated with an impinging jet fire, and it is this issue that this work seeks to address. The model presented here is currently restricted to horizontal natural gas jet fires impinging on a cylindrical target.

THE SPADEADAM TESTS

Extensive details of the experimental procedures and results are given in references 1 and 2. The purpose of this section is to provide a brief overview of the particular measurements pertinent to the development of the model described subsequently.

TABLE 1  
Categorisation of Natural Gas Flame Types in Spadeadam Tests

Flame Type	Orifice Diameter (mm)	Static Pressure (bar)	Mass flow (kg/s)	Release Velocity (Mach)
MB	152	0.02	3	0.4 - 0.5
MC	152	1	8.5	1.2 - 1.3
MD	75	11	8.5	2.2
ME	20	60	3	3.2

A schematic of the natural gas impingement tests is shown in figure 1: Natural gas was released from a discharge platform, designed to permit release at either 1.5 m or 3 m above the ground. Four types of release conditions were used - these are summarised in table 1. Two types of target were used for the tests, a 0.94 m diameter pipe (a 16 m long section of main supply pipe), and a 2.17 m diameter tank (a disused LPG storage vessel, 8.77 m in length). Both targets were mounted on pillars such that their centres were 3 m off the ground. Thus gas could be released at the same vertical height as the target centre, or 1.5 m below the target. Whilst the target position remained fixed, the discharge position could be altered, so that the horizontal separation between discharge point and the target could be varied. Tests were carried out for horizontal separations of 9 m, 15 m, 21 m and 28 m.

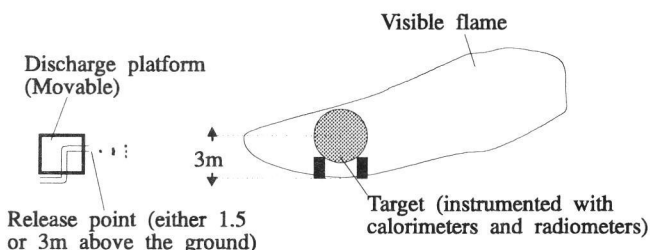


FIG.1 - Schematic of experimental layout in Spadeadam impingement tests

The tank target and pipe target were instrumented for heat flux and temperature measurement. The response time of the radiometers was comparable to the length of the test (taking 68 s to reach 98% of full response). Thus values of radiation calculated from the measured test data were subject to the error associated with extrapolation to infinite time. The response times of the calorimeters were of the order of 30 ms and readings were averaged over time periods during the experiment when the flame was deemed to be steady. Both the calorimeters and radiometers were cooled during the impingement tests and kept at a constant temperature of about 323K, although the remainder of the target was heated by as much as 200 degrees in excess of this value. In a real life situation, as the target heats up it will receive less net flux from the flame; this is because i) the convective heat flux transfer from the flame to the target is proportional to the difference between the bulk jet fire kinetic temperature and the target temperature and ii) the radiative emission of the surface will increase with the fourth power of the surface temperature (in K). Because in the Spadeadam tests, the calorimeters and radiometers are kept at a constant low temperature, the measured fluxes are conservative in respect of the net heat flux which would be impinging on a target in a real-life scenario and thus the model developed in this work is also conservative in this regard. To illustrate this point, a steel tube can be heated up to 1000°C after 20 minutes in a jet fire<sup>6</sup>. If the radiative and convective components of the incident flux are assumed to be approximately equal, then for a jet flame at 1400°C, the net flux received by the tube at 1000°C would be approximately 40% of that which would be received by a tube at room temperature. Also, in contrast to the calorimeters and radiometers in the experiments, a real target will also reflect a certain amount of incident radiation, thus making the test results additionally conservative with respect to a real situation.

IMPINGEMENT PROBABILITY

Carsley has used a colour image analysis system to study videos of various large-scale releases and has developed a predictive model for the probability of a flame existing in a given region of space<sup>5</sup>. In applying the probability model to a cylindrical target, the target was considered not to modify the flow field of the flame in any way and the probability of impingement was thus calculated at various points on the surface of the cylinder, and a contour map of probability was generated.

Figure 2 shows a comparison between measured total flux (in  $\text{kW m}^{-2}$ ) and predicted impingement probability (%) for an MD type natural gas flame, with a tank target located 21 m from the release point. Contour maps were produced using the AGL/GRIDS library of FORTRAN subroutines (version 6.0, which forms part of the UNIRAS package - Uniras A/S Søborg, Denmark). In the target development of figure 2, the surface is "opened out" so that a circumferential distance around the target of zero corresponds to the front of the target and a circumferential distance round the target of +3.45 m or -3.45 m corresponds to the back of the target (the target radius is 1.1 m). The region of 100% impingement probability can be seen to correspond approximately to the area with the highest heat flux.

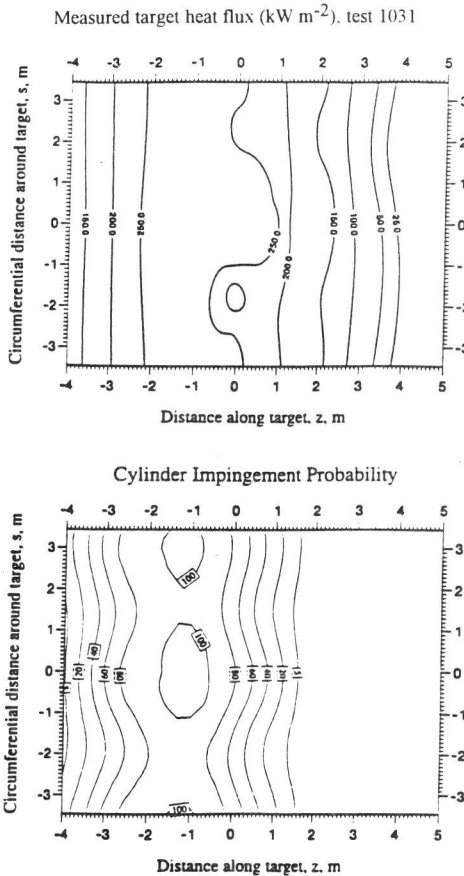


FIG. 2 - Measured target heat fluxes and flame impingement probability (%) for test 1031 (MD type flame; Tank target 21m from release; 1.5 m release height)

A flux of  $50 \text{ kWm}^{-2}$  corresponds very approximately to the visible extent of the flame. The flame therefore extends beyond the region in which it is predicted to exist based on the assumption that the target does not affect the flame; it is apparent that the target does modify the flow field of the flame, causing it to spread around the target - this needs to be accounted for in an adequate model. It was also observed on other tests, with the target close to the release position, that the maximum flux occurs on the back of the target - this can be rationalised by considering that since more of the flame is behind the target than in front of it, the rear of the target will receive more radiation. The radiometer readings bear this out (see figure 3 below). Thus, while impingement probabilities can provide a basis for a model for heat flux distribution, it is clear therefore that account needs to be taken of the flame spread induced by the target, as well as a separate treatment of convective and radiative flux.

RADIATIVE FLUX

The limited number of radiometers on the surface of the targets did not permit separate contour plots of radiative flux to be plotted. The series of tests on MD flames provided the most comprehensive set of radiometer readings. Figure 3 shows the radiation incident on the front and rear of the target as a function of horizontal distance from the release point. It can be seen that (apart from one of the points at 28 m when wind led to a lack of steady impingement), the radiation incident on the front of the target increases with distance from the source. The flame lift-off position for an MD flame (i.e. the average start position of the luminous yellow flame), is typically about 11.8 m from the source.

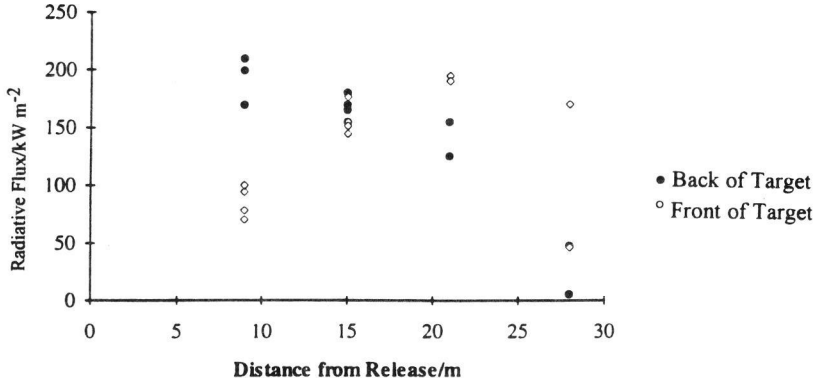


FIG. 3 - Measured radiometer readings for MD type flame natural gas impingement tests

However, the radiation to the front of the target does not apparently decay to zero at lower separations than this. This is because of the region of blue flame in front of the luminous region where molecular emission dominates over soot emission. The blue flame region needs to be accounted for in the modelling. As anticipated, the radiation incident on the back of the target decreases monotonically with distance from the source.

The radiative heat flux density ( $\text{kWm}^{-2}$ ) for an infinitesimal area of receiving surface in the flame is given by

$$\dot{q}_{rad} = \alpha \sigma T_{flame}^4 \tag{1}$$

where  $\sigma$  is the Stefan-Boltzmann constant ( $5.671 \times 10^{-11} \text{ kW m}^{-2} \text{ K}^{-4}$ ),  $\alpha$  is the emissivity coefficient and  $T_{flame}$  is the flame temperature in K. The net radiative transfer between flame and target will also contain a term for the emission of the surface. However, since the calorimeters are kept at a constant temperature, the fourth power of which is insignificant as compared to the fourth power of the flame temperature, then this term can be ignored. In

this work, the flame is treated as isothermal; it is possible to address spatial variations in temperature using zoning methods, or stochastic Monte Carlo approaches<sup>7,8,9</sup>. However, such methods are considerably more computationally demanding than is warranted here, and moreover require an extremely accurate description of the temperature field. The presence of the target may be expected to lead to enhanced mixing at the rear stagnation point and consequently a higher local flame temperature. Such an effect is, however, not considered here.

If the flame is considered to be an arbitrary geometrical shape, homogeneous with respect to temperature and soot concentration, consider the radiation received by an element of receiving surface,  $dA$ . The emissivity,  $\alpha$ , is given by<sup>7,8</sup>

$$\alpha = \iiint_V \frac{K \cos(\theta) \exp(-Kr)}{\pi r^2} dV \quad (2)$$

where the integral is over the volume of flame in front of the receiving area (i.e. where  $|\theta| \leq \pi/2$ )  $r$  is the distance from the receiving surface to the elemental volume of flame,  $dV$ , and  $\theta$  is the angle between the normal to the receiving area and the line joining the receiving surface to the elemental volume. The above triple integral may then be solved numerically - indeed this is the approach adopted by Tunc and Venart in calculating the radiation to a horizontal cylinder in an engulfing pool fire<sup>9</sup>. We adopted a slightly different approach and treated the surface of the flame as a black body at the flame temperature and focused on absorption of radiation by the gas in this hypothetical situation. The absorptivity of the gas thereby calculated can (using Kirchoff's law) be equated to the gas emissivity for the real situation. This method is more numerically tractable, since only a double integral over the flame surface is required.

For the purposes of calculating the emissivity, the flame was treated as having an instantaneous cylindrical shape (fig 4). Reference 4 contains a series of correlations for the position of the end point and lift-off point of the visible flame as a function of both the release conditions and wind. To the length of the cylinder calculated from the correlations of ref 4,  $R_L$ , was added an arbitrary correction factor,  $D_{blue}$  for the region of blue flame between the release point and the start of the luminous region. In reference 4, the flame was treated as a truncated cone - the radius of the cylinder in the present model was taken to be the maximum radius of that cone,  $R_{MAX}$ . In figure 4,  $s$  is the shortest distance from a given elemental area of the target (with surface normal,  $n$ ) to the line joining the visible lift-off point to the flame end. As Carsley's flame impingement probability model has demonstrated, however, flames do not have constant shape and volume, but instead the existence of flame at a particular point is intermittent and is more appropriately described as a flame probability. On this basis, the emissivity,  $\alpha$ , of the elemental area of target surface is then assumed to have the form

$$\alpha = p\alpha_{axis} + (1 - p)\alpha_{edge} \quad (3)$$

where  $\alpha_{axis}$  is the emissivity calculated as if the elemental surface were on the axis of the cylinder,  $\alpha_{edge}$  the emissivity calculated as if the elemental surface was on the edge of the cylinder,  $p$  is the impingement probability

and  $\gamma$  is a factor which describes the attenuation of radiation outside the cylinder. This analysis is equivalent to treating the flame as an ensemble of cylinders. The attenuation parameter,  $\gamma$ , is given by

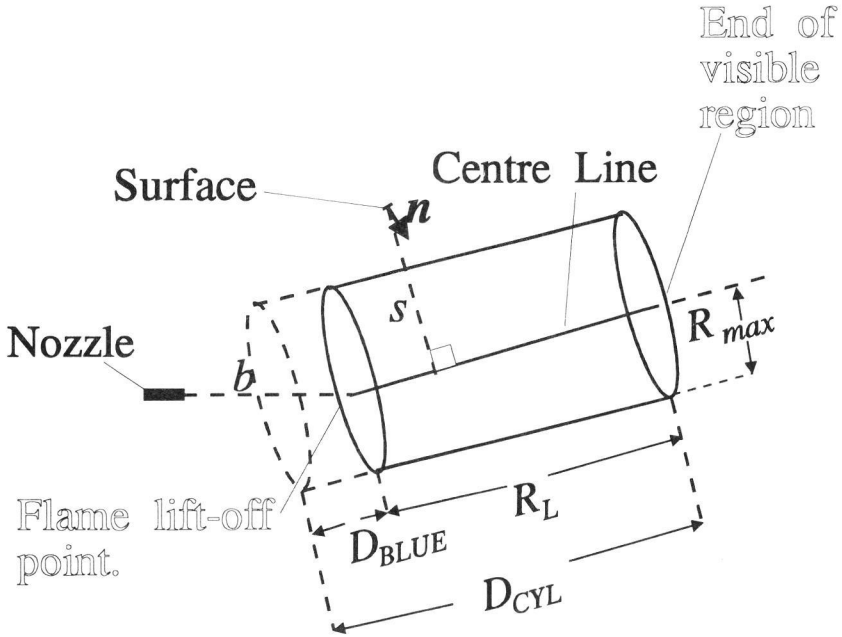


FIG. 4 - The model used in this work for calculation of radiation received by element of surface

$$\begin{aligned} \gamma &= 1 & s \leq R_{MAX} \\ \gamma &= \frac{2}{\pi} \sin^{-1}(R_{MAX} / s) & s > R_{MAX} \end{aligned} \quad (4)$$

The 2D integration required to calculate  $\alpha_{axis}$  and  $\alpha_{edge}$  was performed numerically by dividing the top, bottom and sides of the cylinder into 100x100 segments and using the trapezium rule.

The parameters that provided the best fit of the model to experimental values are  $K=0.19 \text{ m}^{-1}$  (for all natural gas flames),  $D_{blue}=0.39b$  (for all natural gas flames), where  $b$  is the lift off length and  $T=1300^\circ\text{C}$  (MC flame),  $T=1360^\circ\text{C}$  (MD flame),  $T=1400^\circ\text{C}$  (ME flame). The sub-sonic MB type flames were not parametrised directly, but the apparent trend for temperature versus nozzle exit velocity, suggests  $1250^\circ\text{C}$  as an appropriate flame temperature for MB type flames. A comparison of predicted and mean measured radiative flux for MC flames is given in table 2; the model can be seen to give results in reasonably good agreement with experiment.

**TABLE 2**  
**Predicted and measured radiative heat fluxes from MC type natural gas flames**

Distance from Release (m)	Target	Release Height	Predicted Radiative Flux kWm <sup>-2</sup>		Measured Radiative Flux kWm <sup>-2</sup>	
		(m)	Front	Back	Front	Back
9	Pipe	3	112.6	188.1		
9	Tank	3	76.5	188.1	70	177
15	Pipe	1.5	154.4	174.2	156	165
15	Tank	1.5	140.9	177.1	161	168
21	Pipe	1.5	185.5	183.2	187	150
21	Tank	1.5	187	186.7		

The value of K differs from the value of 0.7m<sup>-1</sup> for a methane flame used in calculations by Drangsholt and Wighus<sup>10</sup> - this latter value would considerably overestimate the optical thickness of the flame in respect of the Spadeadam tests, although it should be borne in mind that spectral emission will mean that a single effective grey gas emission coefficient, K, is unlikely to be applicable for both small and large-scale flames. The lift-off distance, b, calculated from ref 4 is typically about 10.5 m for an MC type flame and 12 m for an MD type flame, although the exact value depends on the wind. (and the lift-off position will be intermittently less than this). The question must be asked as to whether it is reasonable for the MD type flame to be both hotter and have a larger blue flame region than the MC type flame. The release velocity is much greater for the MD type than for the MC type (table 1). Ricoh and Spalding<sup>11</sup> suggest that for a turbulent jet, radial mass flow across a flame is proportional to the square root of the jet momentum flux. On this basis, it can be therefore be argued that a faster jet will entrain more air. One might expect faster air entrainment to lead to both a hotter flame and a more significant blue flame region which is totally consistent with the trends observed in the parameter sets. Also the temperatures for the model are consistent with values measured during the tests.<sup>12</sup>

FLAME SPREAD AND CONVECTIVE FLUX

The convective heat flux density (kWm<sup>-2</sup>) for the flame directly impinging on the target is given by

$$\dot{q}_{conv} = h(T_{flame} - T_{target}) \tag{5}$$

where h is the convective heat transfer coefficient (kW m<sup>-2</sup>K<sup>-1</sup>) and T<sub>flame</sub> and T<sub>target</sub> are the flame and target temperatures, respectively. To use a different flame temperature for the convective heat transfer and the radiative transfer would be inconsistent and unrealistic and so the same temperatures were adopted for each flame as described for the radiation model. While the target itself was allowed to heat up, the calorimeters were maintained at around 323K - this therefore is the appropriate value for T<sub>target</sub>.

Comparison of the experimental results with predictions for the impingement probability model (e.g. fig. 2) lead to the conclusion that the target *does* modify the flow field around it. A two-dimensional representation of a flow hitting a target is shown in figure 5. A jet flame of streaming velocity, u, impinges directly on an object.

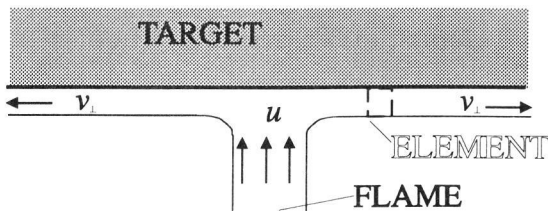


FIG. 5 - Model for spread of flame over surface of impinged object

After impact, a spreading boundary layer has velocity of  $v_{\perp}$  normal to the original direction of the flow. It is assumed in this work that the spreading boundary layer is sufficiently thin that any radiative transfer from the spreading layer to the surface may be ignored. This assumption would be invalid if the spreading layer were optically thick. Consider the element of the spreading boundary layer shown in figure 5: the element is moving from left to right in the figure with speed  $v_{\perp}$ . For the element the relation

$$\text{Rate of heat loss} = \text{Rate of heat loss to surroundings} - \text{Chemical heat production rate} \quad (6)$$

will be true (as indeed will be the case for every other point of the flame). If it can be assumed that the reaction has already gone to completion in the elemental volume of the spreading layer, then the second term on the RHS of equation (11) can be ignored and the following expression may be written for the temperature

$$\frac{d\Delta T}{dt} = -\psi\Delta T \quad (7)$$

where  $\Delta T = T_{\text{flame}} - T_{\text{target}}$  and  $\psi$  is a constant. This equation (which is merely Newton's law of cooling) contains similar information to equation 5 and it would be tempting to equate  $h$  to  $\psi$  multiplied by the specific heat of the material in the elemental volume. This temptation must be resisted because equation (7) describes heat loss to the surrounding air as well as to the surface. Equation (7) may be rewritten in the form

$$\Delta T = \Delta T_0 \exp(-\psi t) \quad (8)$$

where  $t$  is now the time since the reaction went to completion and  $\Delta T_0$  the difference between the bulk flame temperature and the target. The time,  $t$ , is given by

$$t = x / v_{\perp} \quad (9)$$

where  $x$  is the distance from the point at which the reaction goes to completion and equation (8) may be rewritten

$$\Delta T = \Delta T_0 \exp(-\psi x / v_{\perp}) = \Delta T_0 \exp(-\omega x) \quad (10)$$

where  $\omega$  is an adjustable parameter having units  $\text{m}^{-1}$ .

Refocussing on impingement on the tank and pipe targets, the relationship between  $u$  and  $\omega$  depends on the geometry of the impinging object. Thus one might expect  $\omega$  for the spread around the target to be less than  $\omega$  for the spread along the target. An expression for the convective heat transfer incorporating spread can be written:

$$\dot{q}_{\text{conv}} = h\Delta T_0 (p + (1-p)\gamma_1\gamma_2) \quad (11)$$

where  $p$  is the impingement probability and

$$\gamma_1 = 1 \quad x_{\text{round}} \leq R_{\text{max}} \quad (12)$$

$$\gamma_1 = \exp(-x_{\text{round}} \omega_{\text{round}}) \quad x_{\text{round}} > R_{\text{max}}$$

$$\gamma_2 = 1 \quad x_{\text{along}} \leq R_{\text{max}} \quad (13)$$

$$\gamma_2 = \exp(-x_{\text{along}} \omega_{\text{along}}) \quad x_{\text{along}} > R_{\text{max}}$$

$x_{\text{along}}$  is the distance along the cylinder (i.e. parallel to the axis of the cylinder) from the point at which the flame centre line (i.e. the line joining the lift off point to the end of the visible flame) intersects it and  $x_{\text{around}}$  is the distance around the cylinder from the nearest point of intersection of the centre line (the centre line will intersect twice or not at all). The model also makes the assumption that the flame can spread for a distance of  $R_{\text{max}}$  before the chemical heat production term becomes zero. Although the choice of  $R_{\text{max}}$  for this purpose is arguably

somewhat *ad hoc*, it is consistent with  $R_{max}$  as the defining length scale for the flame width and moreover can be justified *a posteriori* by the ability of the model to fit the data shown below. If the centre line does not intersect the cylinder, then clearly the spread of flame over the cylinder surface would be further attenuated and the "(1-p)" term in equation (11) must be multiplied by an additional attenuation factor to reflect this:

$$\gamma_3 = \exp(-2.3r_{miss} / R_{max}) \quad (14)$$

where  $r_{miss}$  is the closest point from the centre line to the surface. The factor of 2.3 is chosen such that  $\gamma_3$  is 0.1 when  $r_{miss} = R_{max}$ .

This analysis is valid only for the flame impinging the target normal (or approximately normal) to the target surface as in figure 5; a model for an arbitrary angle of impingement would have to allow for the fact that the surface boundary layer would not necessarily have the same velocity to the left and right of the impingement point.

For implementation of the model, parameters are required for  $h$ ,  $\omega_{along}$  and  $\omega_{around}$ . The convective transfer coefficient is generally interpreted in terms of a dimensionless parameter called the Nusselt number:

$$h = \frac{k}{D} Nu \quad (15)$$

where  $k$  is the thermal conductivity of the flame, and  $D$  is the characteristic dimension of the surface (in this case the diameter of the cylinder). The problem is then to determine the Nusselt number. For problems such as forced convection to a flat plate, a fairly rigorous detailed analysis can be made of the processes that occur in the boundary layers. These are given in any standard heat transfer text (e.g. Chapman<sup>13</sup>). The problem is far more complex for forced convection to cylinders where, for turbulent flow, the boundary layer separates from the cylinder at about an angle of 110° around the cylinder from the forward stagnation point, consequently the heat transfer coefficient actually varies around the cylinder!

As the impingement probability model demonstrates, the position of the flame in a jet fire is not static - the assumption has therefore been made for modelling purposes that this variability will smear out any local variance of the heat transfer coefficient around the cylinder, allowing an average value of  $h$  to be used. Various correlations for the average Nusselt number around the cylinder exist, with the most reliable being due to Zhukauskas<sup>14</sup> and Churchill and Bernstein<sup>15</sup>. The Nusselt number is a function of two other dimensionless groups, the Prandtl number and the Reynolds number.

$$Nu = f(Re, Pr) \quad (16)$$

The Prandtl number is the balance of momentum flux to thermal flux for the material comprising the flame and the Reynolds number gives the balance of the inertial forces to the viscous forces in the relationship

$$Re = \frac{Du}{\nu} \quad (17)$$

where  $D$  is the characteristic dimension of the surface in m (i.e. the diameter for a cylinder),  $u$  is the streaming velocity of the hot gases comprising the flame ( $m\ s^{-1}$ ) and  $\nu$  is the kinematic viscosity of the hot gases comprising the flame ( $m\ s^{-2}$ ). If the Prandtl number is assumed to remain fairly constant in the flame, then a relationship of the sort

$$h \propto u^m \quad (18)$$

might realistically be anticipated where  $m$  would be expected to be between zero and unity on the basis that this is the range of power for the Reynolds number in empirical correlations of the Nusselt number. Further to this,  $u$  in jets is commonly taken to be inversely proportional to the distance from the release position<sup>16,17</sup> thus a relation

between  $h$  and horizontal distance from the release may be proposed:

$$h = h_o R_D^m \tag{19}$$

where  $h_o$  is the convective heat transfer coefficient at the end of the visible region of flame, and  $R_D$  is the dimensionless horizontal distance of a given point from the release given by

$$R_D = \frac{D_{hoz}}{R_L + b} \tag{20}$$

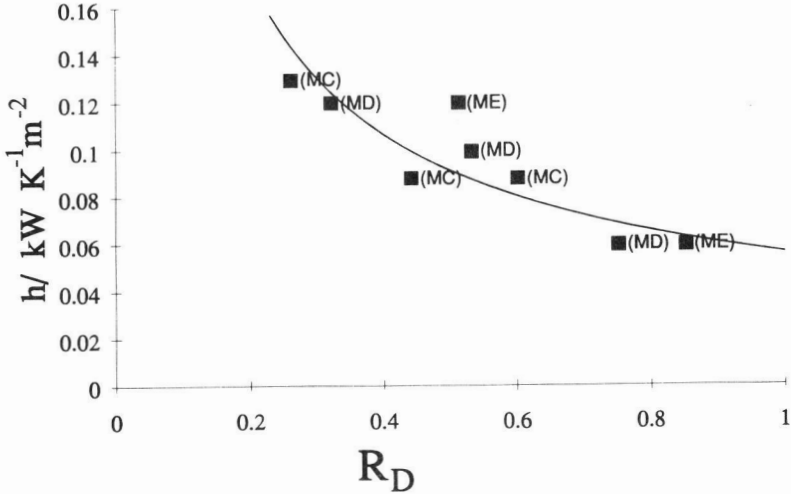


FIG. 6 - Convective heat transfer ( $h$ ) versus dimensionless horizontal distance from release point,  $R_D$ . Best fit value for selected tests (■); Correlation (-)

where  $b$  and  $R_L$ , both in m, are the flame lift-off and flame length parameters respectively defined in figure 4, and  $D_{hoz}$  is the horizontal distance of a given point from the release in m.

A representative selection of impingement tests for sonic releases were then subjected to closer scrutiny. For each test, a value of  $h$  was chosen which, when combined with the radiation model, gave the best fits to experimental plots of impinged area versus heat flux. Unsurprisingly, when plotted against  $R_D$ , the values of the best fit convective heat transfer coefficient show considerable scatter (figure 6). However, a clear trend can be discerned for  $h$  to decrease with  $R_D$ . It is also not possible to discriminate between the different release types, which has the advantage that a single correlation can be used for all of the data. Fitting the data to equation (19) gave the line shown in figure 6, with parameters of  $h_o=0.06 \text{ kW K}^{-1} \text{m}^{-2}$  and  $m=0.7$ . These parameters are valid for all natural gas flames in the test.

The spread parameters were found to be given by

$$\omega_{around} (\text{m}^{-1}) = 0.55 R_D^m \tag{21}$$

$$\omega_{along} (\text{m}^{-1}) = 1.1 R_D^m \tag{22}$$

It should be recalled that a lower value of  $\omega$  gives rise to more spread. Consequently equations (21) and (22)

suggest that the closer the target is to the release, the more spread will occur and also the spread around the target will be greater than the spread along the target. The data were not extensive enough to determine different parameters for the tank and the pipe, although intuitively one might not expect the spread for both to be exactly the same.

A criticism which can be levelled at the type of correlation used in equation (19) is that  $h$  would be infinite at the release point. If the limit of validity of the model is restricted to the visible region, the anomaly therefore does not matter. For modelling non-lifted jets it is recommended that a maximum value of  $h=0.16\text{kWm}^{-2}\text{K}^{-1}$  be used.

#### SELECTED RESULTS

A comparison of selected measured and predicted results are shown in figures 7 through 11. The tests were chosen as a representative subset of all the Spadeadam tests and cover a wide range of release types and target configurations. Figures 7 to 10 show a comparison of contour plots of predicted and measured heat fluxes. Figure 11 shows for a given value of flux density, the amount of target surface area having a greater or equal flux density. The solid line is the prediction using the model, and the dashed line the measured value.

In all four examples, the model is able to approximately reproduce the main features of the test results, especially in respect of the impinging area versus flux (figure 11), which is of vital import for the design of structures. In test 2031 (figure 8) the flame was blown significantly off the centre of the target. The wind correlation of reference 4 correctly predicts this and the flux model gives an accurate (although slightly conservative) account of the flux distribution. In tests 1070 (figure 10) and 1032 (figure 11), the flame is blown slightly off the centre of the target. The centre of the target contained more calorimeters per unit area than the region on the left part of the target, permitting a more accurate resolution of the flux distribution. The apparent asymmetry in the contour plot of the target development arises as a direct consequence of this. As expected, asymmetry is not observed in the model predictions.

#### CONCLUSIONS

A model has been developed which is able to predict the total net heat flux to a cylindrical object in an impinging natural gas jet fire. The model was parameterised for sonic releases and works acceptably well for these. The model also works for sub-sonic releases (type MB). The model in its present form is strictly valid only for horizontal distances for the release point greater than the flame lift-off and less than the flame end. The model for impingement assumes the flame hits the surface approximately along its normal in the manner of figure 5. The flame spread will be different to the left and right of the impingement point if this criterion is not (approximately) fulfilled. The model in its current form is valid only for cylinders. Since different spread parameters for the pipe and tank could not be discriminated, it may be asserted that they are valid for cylindrical targets of diameter up to the flame width. Extension of the model to flat plates, "I" sections or other shapes of engineering interest would require new spreading parameters and possibly a correction for augmented flame temperature due to additional turbulent mixing on impingement.

Nicolette and Larson<sup>19</sup> have, however, suggested a model whereby thermally massive objects can cool the region of the flame directly impinging upon them, the reduction in flame temperature thereby lowering the incident radiation to the surface. Such effects can be ignored for natural gas flames because the length scale over which the target can thermally influence the flame is likely to be small compared to the path length of the radiation. Moreover, in this work, the flame temperatures used to fit the model are consistent with the experimental temperature measurements. This factor may, however, need consideration for flames of higher hydrocarbons, although errors caused by neglecting blockage would make the model more conservative.

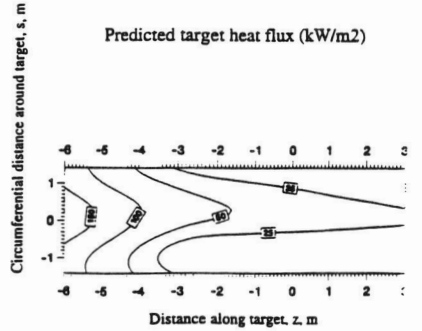
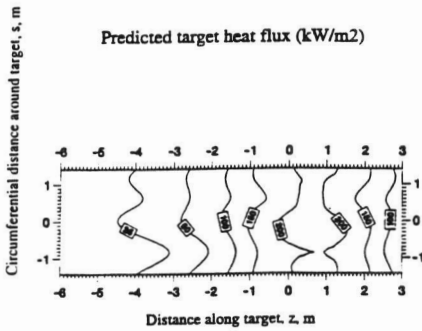
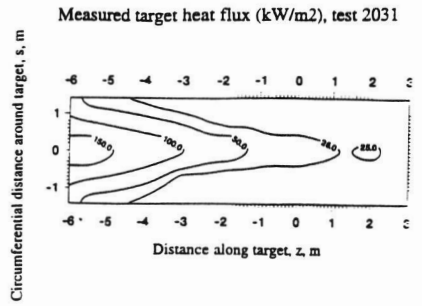
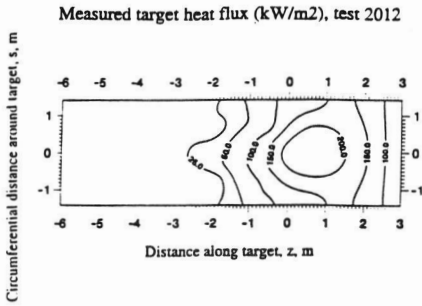


FIG 7. Measured and predicted contour map of flux density for test 2012(MB type flame, pipe target 15m from release.)

FIG 8. Measured and predicted contour map of flux density for test 2031(MC type flame, pipe target 28m from release.)

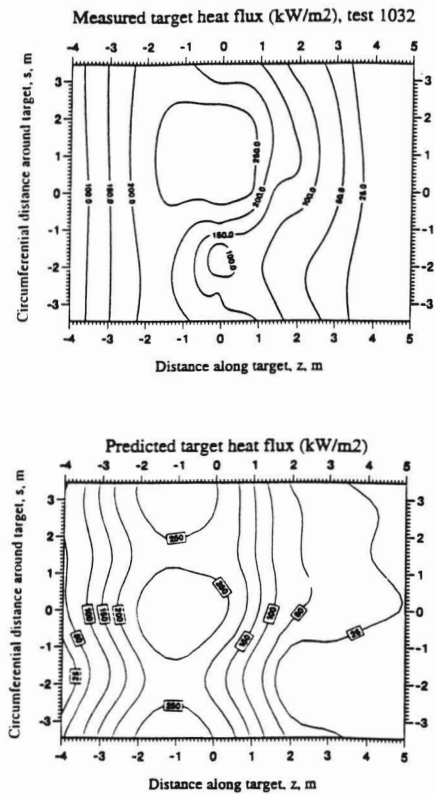


FIG 9. Measured and predicted contour map of flux density for test 1032(MD type flame, pipe target 21m from release.)

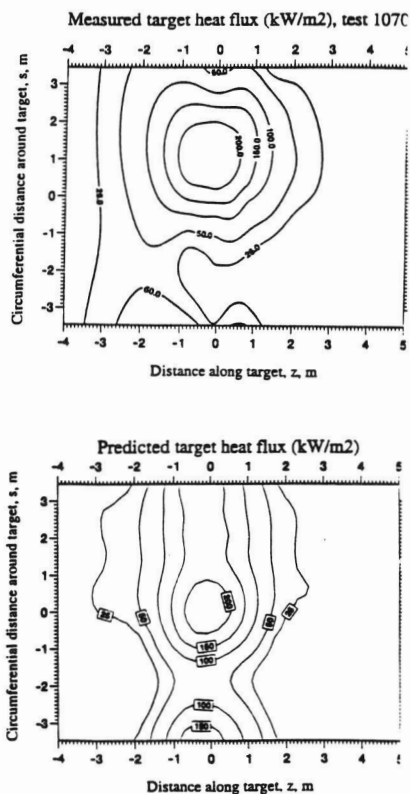


FIG 10. Measured and predicted contour map of flux density for test 1070(ME type flame, pipe target 15m from release.)

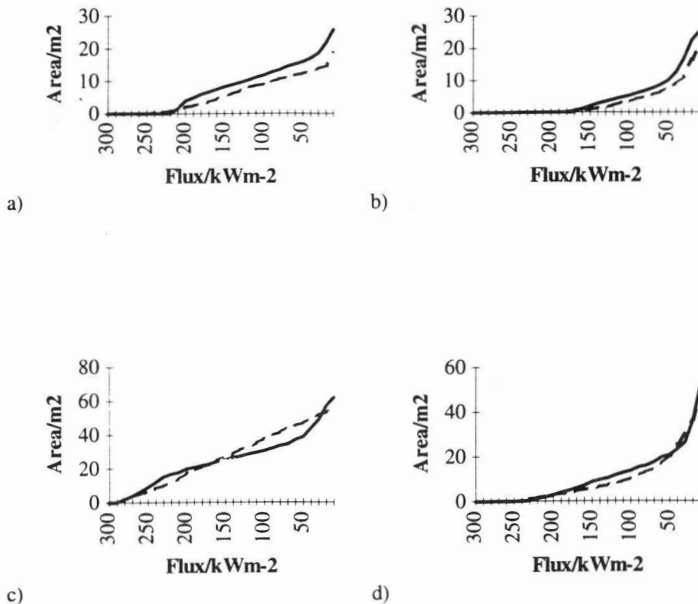


FIG. 11. Impinged area with a given or greater heat flux density versus flux density. Predicted (—) and measured (-----) values for tests 2012 (a), 2031, (b), 1032(b) and 1070 (d).

REFERENCES

1. J.N. Davenport, J.F. Bennett, L.T. Cowley and J.J. Rowson, "Large Scale Natural Gas and LPG Jet Fires. Data Reports" TNER.91.023 to TNER.91.195 inclusive, Shell Research Limited, 1991.
2. J.F. Bennett, L.T. Cowley, J.N. Davenport and J.J. Rowson, "Large Scale Natural Gas and LPG Jet Fires Final Report to CEC ", TNER.91.022, Shell Research Limited, 1991.
3. G.A. Chamberlain, Chem. Eng. Res. Des. 65, pp299-310, 1987.
4. A.D. Johnson, H.M. Brightwell and A.J. Carsley; Trans. I. Chem. E. 72(B), pp 157-166, 1994.
5. A.J. Carsley, to be presented at 2nd European Conference on Major Hazards, On and Offshore, UMIST, Manchester, 24-26 October 1995.
6. M.A. Persaud and L.C. Shirvill in preparation for Proc. Safety Env. Prot.
7. R. Siegel and J.R. Howell, "Thermal Radiation Heat Transfer", Hemisphere, Washington, 1992.
8. H.C. Hottel and A.F. Sarofim, "Radiative Transfer", McGraw-Hill, New York, 1967.
9. M. Tunc and J.E.S. Venart, "Incident Radiation from an Engulfing Pool Fire to a Horizontal Cylinder - Part I", Fire Safety Journal, 8, pp81-87, 1984/1985.
10. G. Drangsholt and R. Wighus, "Test Conditions for an Impinging Jet Fire", SINTEF report STF25 A900197, 1992.
11. F.P. Ricoh and D.B. Spalding, "Measurements of Entrainment by Axisymmetrical Turbulent Jets", J. Fluid Mech., 11, pp21-32, 1961.
12. J.N. Davenport, unpublished data, Shell Research Ltd.
13. A.J. Chapman, "Heat Transfer", Macmillan, 1984.
14. A. Zhukauskas, "Heat Transfer from Tubes in Crossflow", Adv. Heat Transfer, 8,, p93, 1972
15. S.W. Churchill and M. Bernstein, "A Correlating Equation For Forced Convection from Gases and Liquids to a Circular Cylinder in Crossflow", Trans. ASME, 94, p300, 1977
16. A.D. Birch, D.R. Brown, M.G. Dodson and F. Swaffield, "The Structure and Concentration Decay of High Pressure Jets of Natural Gas", Com. Sci and Tech. 36 pp 249-261, 1984.
17. A.D. Birch, DJ Hughes and F. Swaffield, "Velocity Decay of High Pressure Jets", Com. Sci and Tech. 52 pp 161-171, 1987.
18. E. Achenbach, "The Effect of Surface Roughness on the Heat Transfer Coefficient form a Circular Cylinder to the Cross-flow of Air", Int. J. Heat Mass Transfer 20, pp 359-369 (1977).
19. V.F. Nicolette and D.W. Larson, "The Influence of Large Cold Objects on Engulfing Fire Environments" in "Heat and Mass Transfer in Fires" J.G. Quintiere, L.Y. Cooper eds.-Proc. AIAA/ASME Thermophysics and Heat Transfer Conference, 1990